# Self-Adaptive Stabilization Control of a Rotary Pendulum using Nonlinearly-Scaled Model-Reference Gain-Adaptation Law

**Omer Saleem\*, Fahim Gohar Awan\*\*, Samia Mahmood\*, Sheroze Liaquat\*, Hamza Yousuf\***

*\*Department of Electrical Engineering, National University of Computer and Emerging Sciences,
Lahore, Pakistan (e-mail: omer.saleem, samia.mahmood, shahroze.liaquat, hamza.yousuf@nu.edu.pk)
\*\*Department of Electrical Engineering, University of Engineering and Technology,
Lahore, Pakistan (e-mail: fawan@uet.edu.pk)*

**Abstract:** This article presents the formulation of a novel self-adjusting model-reference-adaptive-control law to enhance the position-regulation and disturbance-rejection capability of Rotary-Inverted-Pendulum (RIP) systems. Initially, the baseline Linear-Quadratic-Regulator (LQR) is augmented with an online gain-adjustment law that modifies the state-compensator gains via pre-calibrated state-error dependent dissipative and anti-dissipative functions to improve the system's position-regulation capability. To further enhance the controller's robustness against exogenous disturbances, the baseline LQR is instead retrofitted with the proposed self-adjusting model-reference-adaptive-system that employs Lyapunov function to formulate a stable online state-compensator gain-adjustment law. The adaptability of the model-reference gain-adjustment law is increased by dynamically modifying the adaptation-gain of self-tuning law via a pre-calibrated Gaussian scaling function that is driven by the system's state-error variations. The hyper-parameters associated with the aforementioned adaptive control systems variants are empirically tuned by minimizing an auxiliary quadratic cost function that captures the classical-state-error and control-input variations. The proposed adaptive control system variants are examined in the physical environment by conducting credible real-time hardware experiments on QNET Rotary Pendulum Board. The experimental outcomes validate the superior robustness of the self-adjusting model-reference-adaptive-control system against the bounded exogenous disturbances and modeling-errors.

*Keywords:* Linear-quadratic-regulator, self-tuning control, model-reference-adaptive-controller, Lyapunov function, Gaussian scaling function, rotary pendulum.

## 1. INTRODUCTION

The Rotary-Inverted-Pendulum (RIP) system has garnered a lot of traction as a standard benchmark platform for the development and validation of advanced control systems for under-actuated mechatronic systems (Li et al., 2013; Boubaker, 2013). The theory of RIP stabilization is extensively used in the stabilization of humanoid robots, bio-mechatronic systems, rockets, aircrafts, submarines, unmanned-air-vehicles, and satellites, etc (Zhang et al., 2014). The RIP is an inherently unstable, highly nonlinear, and under-actuated system which makes it an ideal platform to emulate the behaviour of the aforementioned systems in real-time (Grilti et al., 2018). However, owing to its kinematic instability and nonlinear dynamics, synthesizing an agile regulatory control mechanism for such a system to enhance its robustness against bounded exogenous disturbances and parametric variations is a very challenging control problem (Yu et al., 2008).

### 1.1. Related Work

Rigorous research has been done to develop stable and agile stabilization controllers for the RIP systems (Mahmoud, 2018). Despite their simplicity, the conventional PID controllers lack the degrees-of-freedom to efficiently regulate the system's behaviour under abrupt parametric variations (Bhatti et al., 2015). The intelligent controllers also deliver a reliable and agile control effort. However, synthesizing a reliable set of rules or gathering large sets of training data is a laborious task (Szuster and Hendzel, 2017). Additionally, the neural controllers inevitably put an excessive computational burden on the embedded signal processor (Sefriti et al., 2012). The sliding-mode controllers are renowned for their robust control yield. However, they contribute discontinuous control activity and chattering in the system's time-domain response (Ullah et al., 2019).The Linear-Quadratic-Regulator (LQR) is a state-feedback controller that utilizes the system's nominal state-space model to minimize a quadratic performance index of the system's state-trajectories and control-input to yield stable and optimal control decisions. However, the existence of identification errors and the lack of information regarding the un-modeled intrinsic nonlinearities in the nominal model prevents the generic LQR from effectively rejecting the external disturbances (Ghertemani et al., 2011). Consequently, the control effort is severely affected under parametric variations which cause the pendulum to collapse (Prasad et al., 2014). The identification of time-varying nonlinearities is quite difficult due to the restraints imposed by the system's complex dynamics.

Stable adaptive control systems are widely favored because of their capability to efficiently mitigate the effects of disturbances caused by random faults without deteriorating the system's performance during real-time or mission-critical applications (Bhatti et al., 2018). A well-postulated adaptive system automatically adjusts the critical controller parameters,

by using analytical or logical rules, to enhance the system's robustness across a broad range of operating conditions (Szuster and Hendzel, 2017). The gradient-descent-based adaptation mechanisms, and their modified variants, have been frequently proposed in the open literature for the stable online dynamic adjustment of controller-gains, owing to their quick convergence to local minima (Hanwate et al., 2019). An innovative derivative-based online gain adaptation mechanism has been proposed in (Fisher et al., 2009) to robustify the ship cruise control systems. Fisher's adaptation mechanism is composed of dissipative and anti-dissipative terms that significantly enhance the sensitivity of the parameter adjustment law which in turn strengthens the controller's reference-tracking accuracy (Balestrino et al., 2011). However, ill-postulated iterative algorithms inevitably put a recursive computational burden on the embedded processor. The unbounded growth (or decay) of controller gains causes integral wind-up which leads to actuator saturation and possible system failure. The selection of the parameters associated with the gain-adjustment law is also quite hectic.

The Model-Reference-Adaptive-Controller (MRAC) is a state-of-the-art adaptive control system that enhances the system's reference-tracking accuracy and resilience against exogenous disturbance (Subramaniana and Elumalai, 2016). It employs Lyapunov theory to formulate a stable gain-adaptation law that modifies the controller's controller gains, after every sampling interval (Chen, 2017). The Lyapunov function minimizes the difference between the outputs of the reference closed-loop system (governed by the LQR) and the actual closed-loop system to synthesize an asymptotically-stable online gain-adjustment law. The preset adaptation-gains of the Lyapunov gain-adjustment law must be carefully selected as they are responsible for driving the state-compensator gains to their local-optimum values (Cuong et al., 2013). Firstly, the selection of the adaptation-gains is an ill-posed problem. Secondly, the fixed values of the adaptation-gains fail to address the discontinuities associated with the behavior of the RIP system during its equilibrium-state and perturbed-state (Hassanzadeh et al., 2011). In the equilibrium-state, the RIP encounters undesired limit cycles caused by the mechanical friction that severely affects its postural stability. In the perturbed-state, the intrinsic nonlinearities such as actuator's backlash and force-ripple tend to deteriorate the system's reference tracking performance.

### 1.2. Proposed Methodology

The **main contribution** of this article is the systematic formulation of a nonlinearly-scaled MRAC strategy for an under-actuated RIP system to enhance its position-regulation accuracy and disturbance-rejection capability. The generic LQR is used as the primary fixed-gain state-feedback control scheme. The LQR is augmented with a stable online gain-adjustment law that uses pre-defined meta-rules, in conjunction with the state-error feedback, to vary the controller gains. The novel contributions of this article are postulated as follows:

- Initially, the LQR gains are directly modified online by using Fisher's adaptation mechanism with pre-configured dissipative and anti-dissipative functions (Balestrino et al.,

2011). This controller establishes a baseline for comparison with the proposed controller.
- The architecture of the adaptive controller is evolved by retrofitting the ubiquitous state-space MRAC with the proposed nonlinearly-scaled self-adjusting adaptation-gain law. Where in, the constituent adaptation-gains of the MRAC are dynamically altered, after every sampling-interval, via pre-configured nonlinear scaling functions.
- The nonlinear scaling is done via pre-calibrated zero-mean Gaussian functions that are driven by the system's classical state-error variations. This augmentation eliminates the performance limitations rendered by the fixed adaptation-gains. It increases the controller's degrees-of-freedom which enables the system to quickly transit from perturbed-state to equilibrium-state with minimal fluctuations.
- The aforementioned propositions are justified by benchmarking the performance of the proposed N-MRAC against the fixed-gain LQR and the "Fisher-adaptive" LQR equipped. The comparison is done by conducting credible hardware experiments on the QNET Rotary Pendulum.

The development of the nonlinearly-scaled MRAC (N-MRAC) is the original contributions of this article. The formulation, implementation, and experimental validation of the proposed N-MRAC to enhance the robustness of the RIP system's stabilization controller has not been discussed in the available open literature. Hence, this idea is the main focus of this article. The proposed N-MRAC strategy offers several innovative traits. Firstly, it enhances the adaptability and convergence-rate of the adjusted state-compensator gains which enhances the stabilization controller's robustness against bounded exogenous disturbances. Secondly, the Lyapunov criterion ensures the asymptotic stability of the N-MRAC law (as discussed later in this article). Thirdly, the realization of the nonlinear scaling using the Gaussian function is yet another novel contribution of this article. Apart from being continuous and even-symmetric, this algebraic equation can be solved in a single step which reduces the recursive computational burden on the embedded processor. Hence, it can be easily programmed via modern-day digital computers.

### 1.3. Previous Publications

The preliminaries associated with the proposed system are acquired from the previous works (Saleem and Mahmood-ul-Hasan, 2019; Saleem et al., 2020; Saleem and Mahmood-ul-Hasan, 2021).

The rest of the paper is organized as follows. The system's description is presented in Section 2. The baseline LQR is synthesized in Section 3. The proposed adaptive controller is formulated in Section 4. The proposed control schemes are experimentally evaluated in Section 5. The article is concluded in Section 6.

## 2. SYSTEM DESCRIPTION

The details regarding the hardware setup and mathematical model of the system are presented as follows.

### 2.1. Experimental Setup

The QNET Rotary Pendulum Board, shown in Figure 1, is used in this research to experimentally examine the efficacy of

the proposed control strategies (Ashrafiuon and Whitman, 2011). The system's hardware schematic is shown in Figure 2. The pendulum rod rotates freely about the y-axis. The pivoted end of the rod is coupled to a rotary encoder that measures the rod's pitch angle, denoted as $\theta$. The rod's free end is coupled with a 0.1 kg counter-mass. The angular motion of the rod depends on the rotation of the arm attached to it. The rod is rotated via a DC geared servo motor. The motor shaft is coupled to a encoder that measures the variations in the arm's yaw-angle, denoted as $\alpha$. The clockwise rotation of the rod and the arm is taken as the positive angular movement about their respective axes. The reference value of $\theta$ is fixed at -$\pi$ radians. The initial angular position of the arm, $\alpha(0)$, is selected as its reference. The NI-ELVIS II Data-Acquisition (DAQ) board is used to serially communicate information between the control software and the hardware setup at 9600 bps.



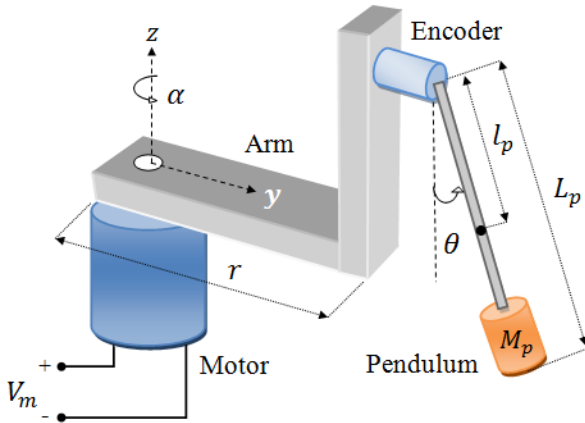Fig. 1. QNET Rotary Pendulum Board.



Fig. 2. Simplified schematic of RIP.

The ELVIS DAQ board acquires the sensor-readings related to the real-time state-variations at a sampling frequency of 1000 Hz. This sampling frequency is chosen due to the small inertia and high agility of the RIP system. A higher frequency resulted in oversampling of the sensor data.The acquired data is serially transmitted to a LabVIEW-based control application (Saleem et al., 2020a). The software is operated on a 64-bit, 1.8 GHz embedded computer with 8.0 GB RAM. The control application's front-end acts as a graphical-user-interface that aids in recording and visualizing the instantaneous variations

in state and control-input variables. The back-end of the application provides a platform to run the custom-built software control application that receives the digitized sensor readings, generates appropriate control signals, and serially transmits the control signals to the hardware setup. The modulated control signals are transmitted to a driver circuit that amplifies them to drive the DC servo motor. The control application is digitally implemented by using the "Block Diagram" tool of the LabVIEW software. The adaptation laws are programmed via C-language in the Math-Script tool.

### 2.2. Mathematical Model

The RIP system's model is derived by using the Euler-Lagrange technique (Jian and Yongpeng, 2011). The system's Lagrangian is computed by evaluating the difference between the system's total kinetic energy and total potential energy in terms of its state-variables ($\alpha$, $\theta$, $\dot{\alpha}$, and $\dot{\theta}$). The computed Lagrangian function is used to acquire the Euler-Lagrange equations. The DC motor's toque, $\tau$, is taken as the input variable. The system's state-variables are taken as the outputs. The frictional forces are neglected due to their negligible contribution. The resulting nonlinear equations of motion are expressed below (Jian and Yongpeng, 2011).

$$\ddot{\alpha} = -\frac{1}{S}\left(rM_p^2l_p^2g(\cos\theta)\theta + J_pM_pr^2(\cos\theta)(\sin\theta)(\dot{\alpha})^2 + (J_p + M_pl_p^2)\tau\right)$$

$$\ddot{\theta} = \frac{1}{S}\left(-M_pl_p(M_pr^2(\sin^2\theta)g - J_eg - M_pr^2g)\theta \right.$$
$$- M_pl_pr(\sin\theta)J_e(\dot{\alpha})^2$$
$$\left. + M_pl_pr(\cos\theta)\tau\right) \qquad (1)$$

such that, $\qquad \tau = \dfrac{K_t(V_m - K_m\dot{\alpha})}{R_m}$

and, $\qquad S = J_p(M_pr^2(\sin^2\theta) - J_e - M_pr^2) - M_pl_p^2J_e$

where, $V_m$ represents the DC motor's voltage signal. The other notations in (1) are described in Table 1. To acquire the linear state-space model, the aforementioned equations are linearized around the point; $\theta = -\pi$ rad., $\alpha = 0$, $\dot{\alpha} = 0$, $\dot{\theta} = 0$, and $V_m = 0$ V. The linear equations of motion are shown below.

$$\ddot{\alpha} = \frac{1}{W}\left(rM_p^2l_p^2g\theta - \frac{(J_p + M_pl_p^2)K_tK_m}{R_m}\dot{\alpha} + \frac{(J_p + M_pl_p^2)K_t}{R_m}V_m\right)$$

$$\ddot{\theta} = \frac{1}{W}\left(M_pl_pg(J_e + M_pr^2)\theta - \frac{rM_pl_pK_tK_m}{R_m}\dot{\alpha} + \frac{rM_pl_pK_t}{R_m}V_m\right) \quad (2)$$

such that, $\qquad W = J_eJ_p + M_pr^2J_ps + M_pl_p^2J_e$

These linear equations are used to derive the system's nominal state-space model.

The general state-space representation of a linear system is expressed in (3) and (4).

$$\dot{x}(t) = Ax(t) + Bu(t) \qquad (3)$$

$$y(t) = Cx(t) + Du(t) \qquad (4)$$

where, $x(t)$ is the state vector, $y(t)$ is the output vector, $u(t)$ is the control-input signal, $\boldsymbol{A}$ is the state matrix, $\boldsymbol{B}$ is the inputmatrix, $\boldsymbol{C}$ is the outputmatrix, and $\boldsymbol{D}$ is the feed-forward matrix. The state-variables of the RIP system are formally expressed in (5).

$$x(t) = \begin{bmatrix} \alpha(t) \\ \theta(t) \\ \dot{\alpha}(t) \\ \dot{\theta}(t) \end{bmatrix} \tag{5}$$

**Table 1. Identification of RIP system parameter**

| Symbol | Description | Value |
|--------|-------------|-------|
| $M_p$ | Mass of pendulum | 0.027 kg |
| $l_p$ | Pendulum center of mass to pivot length | 0.153 m |
| $L_p$ | Length of pendulum rod | 0.191 m |
| $r$ | Length of horizontal arm | 0.083 m |
| $J_m$ | Motor shaft moment of inertia | $3 \times 10^{-5}$ kgm$^2$ |
| $M_{arm}$ | Mass of arm | 0.028 kg |
| $g$ | Gravitational acceleration | 9.810 m/s$^2$ |
| $J_e$ | Moment of inertia about motor shaft pivot | $1.23 \times 10^{-4}$ kg.m$^2$ |
| $J_p$ | Moment of inertia about pendulum pivot | $1.1 \times 10^{-4}$ kgm$^2$ |
| $R_m$ | Motor armature resistance | 3.30 Ω |
| $L_m$ | Motor armature inductance | 47.0 mH |
| $K_t$ | Motor torque constant | 0.028 N.m |
| $K_m$ | Motor back-electromotive force constant | 0.028 V/(rad/s) |
| $\tau_{max}$ | Maximum torque | 0.14 Nm |
| $V_{rated}$ | Motor's rated voltage | ±24.0 V |
| $I_{rated}$ | Motor's rated current | 5.0 A |

The control-input variable of the system is expressed below.

$$u(t) = V_m(t) \tag{6}$$

The nominal state-space model of the QNET RIP system is expressed in (6).

$$A = \begin{bmatrix} 0 & 0 & 1 & 0 \\ 0 & 0 & 0 & 1 \\ 0 & m_1 & m_2 & 0 \\ 0 & m_3 & m_4 & 0 \end{bmatrix}, \qquad B = \begin{bmatrix} 0 \\ 0 \\ p_1 \\ p_2 \end{bmatrix},$$

$$C = \begin{bmatrix} 1 & 0 & 0 & 0 \\ 0 & 1 & 0 & 0 \\ 0 & 0 & 1 & 0 \\ 0 & 0 & 0 & 1 \end{bmatrix}, \qquad D = 0 \tag{7}$$

where,

$$m_1 = \frac{r M_p^2 l_p^2 g}{J_p J_e + J_e l_p^2 M_p + J_p M_p r^2}, m_2 = \frac{-K_t K_m (J_p + M_p l_p^2)}{(J_p J_e + J_e l_p^2 M_p + J_p M_p r^2) R_m},$$

$$m_3 = \frac{M_p l_p g (J_e + M_p r^2)}{J_p J_e + J_e l_p^2 M_p + J_p M_p r^2}, m_4 = \frac{-r M_p l_p K_t K_m}{(J_p J_e + J_e l_p^2 M_p + J_p M_p r^2) R_m},$$

$$p_1 = \frac{K_t (J_p + M_p l_p^2)}{(J_p J_e + J_e l_p^2 M_p + J_p M_p r^2) R_m}, p_2 = \frac{r M_p l_p K_t}{(J_p J_e + J_e l_p^2 M_p + J_p M_p r^2) R_m}$$

As mentioned earlier, the descriptions as well as the numerical values associated with the system's modeling parameters are presented in Table 1 (Quanser, 2019).

## 3. BASELINE LINEAR QUADRATIC REGULATOR

The LQR is a model-based optimal state-space controller. It utilizes the system's linear state-space model to deliver optimal control decisions by minimizing the deviations in the state-trajectories as well as the control input by using an energy-like quadratic performance index (Lewis et al., 2012). The quadratic performance index is given by (8).

$$J_{lq} = \int_0^\infty \left( x(t)^T Q x(t) + u(t)^T R u(t) \right) dt \tag{8}$$

where, $Q$ and $R$ are the state and the control weighting matrices, respectively. The state-weighting matrix is positive semi-definite of the form $Q = Q^T \geq 0$. The control-weighting matrix is positive definite of the form $R = R^T > 0$. The resulting linear optimal control law derived is given by (9).

$$u(t) = -K_{lqr} x(t) \tag{9}$$

such that, $\qquad K_{lqr} = \begin{bmatrix} k_\alpha \\ k_\theta \\ k_{\dot{\alpha}} \\ k_{\dot{\theta}} \end{bmatrix}^T$

where, $K_{lqr}$ is the optimal state-compensator vector, $k_\alpha$ is the proportional-gain associated with $\alpha$, $k_\theta$ is the proportional-gain associated with $\theta$, $k_{\dot{\alpha}}$ is the derivative-gain associated with $\dot{\alpha}$, and $k_{\dot{\theta}}$ is the derivative-gain associated with $\dot{\theta}$. The state-compensator gain-vector, $K_{lqr}$, aids in the optimal placement of the system's closed-loop poles on the left-half side of the complex plane to yield an optimal control effort. The state-compensator gains are calculated offline as shown below.

$$K_{lqr} = R^{-1} B^T P \tag{10}$$

where, $P$ is a symmetric positive-definite co-state matrix. The co-state matrix $P$ is evaluated offline by solving the Algebraic-Riccati-Equation (ARE) expressed in (11).

$$A^T P + PA - PBR^{-1}B^T P + Q = 0 \tag{11}$$

Selecting a unique set of state and control weighting-factors is an ill-posed problem (Okyere et al., 2019). The control weighting-factor $R$ of $J_{lq}$ is selected as unity. The coefficients of the state-weighting-matrix $Q$ are empirically selected by minimizing the auxiliary quadratic cost-function, shown in (12), to acquire a unique set of weighting-factors that deliver optimum position-regulation accuracy.

$$J_2 = \int_0^\infty \left[ \left( e_\alpha(t) \right)^2 + \left( e_\theta(t) \right)^2 + \left( V_m(t) \right)^2 \right] dt \tag{12}$$

where, $\qquad e_\theta(t) = \theta(t) - \theta(0), \qquad e_\alpha(t) = \alpha(t) - \alpha(0)$

The variables $e_\theta(t)$ and $e_\alpha(t)$ are the classical state-error variables representing the difference between the actual and set-point positions of the pendulum's rod and arm, respectively. The value of $\theta(0)$ is preset at $-\pi$ radians (or -180 deg.) in this research. The weighting coefficients of $\left( e_\alpha(t) \right)^2$, $\left( e_\theta(t) \right)^2$, and $\left( V_m(t) \right)^2$ are empirically adopted as unity in the integrand $J_2$. The linearized model of the RIP is used for the offline calibration of the weighting-factors. The tuning is conducted empirically by moving in the direction of descending gradient of the cost function $J_2$ until a unique set of weighting factors that yield the minimum cost is achieved. After every iteration, the cost is evaluated for the new set of coefficients of $Q$. The set of coefficients that yield the

minimum cost are selected. The weighting-coefficients adopted in this research are given in (13).

$$Q = \begin{bmatrix} 38.2 & 0 & 0 & 0 \\ 0 & 52.6 & 0 & 0 \\ 0 & 0 & 5.3 & 0 \\ 0 & 0 & 0 & 2.1 \end{bmatrix}, \quad R = 1 \tag{13}$$

The matrices $Q$ and $R$, selected in (13), are used to solve the ARE expressed in (11). The solution of the LQR problem yields the following state-compensator gains.

$$K_{lqr} = \begin{bmatrix} -6.21 \\ 130.56 \\ -4.22 \\ 17.83 \end{bmatrix}^T \tag{14}$$

The state variables related to the horizontal arm ($\alpha$ and $\dot{\alpha}$) have negative gains. If all the states are zero, except for any one of the states having negative gains, then the control loop will enter positive feedback for a brief moment. Consequently, the control system will push the horizontal arm in same direction, tilting the pendulum's rod backwards and then pushing the arm back to its original position. Pushing the horizontal arm to its original position, without tilting the rod back, will cause the rod to de-stabilize from its vertical position and collapse.

## 4. SELF-ADAPTIVE CONTROL SYSTEM DESIGN

The self-adaptive control system enhances the system's immunity against bounded disturbances. This section presents the design procedure of two self-adaptive control strategies.

### 4.1. Fisher-adaptive Self-tuning Regulator (F-STR)

The process of online gain-adaptation is initiated by employing the "Fisher" adaptation mechanism with pre-calibrated dissipative and anti-dissipative functions (Fisher et al., 2009). It flexibly modifies the controller's state-compensator gains online which enable the controller to respond to a wide range of operating conditions in under-actuated systems (Balestrino et al., 2011). It does not require a priori knowledge of the system's model. Instead, it initiates from the nominal preset values of state-compensator gains and then modifies them online, once after every sampling interval, on the basis of real-time state-error variations. The block diagram of the Fisher-adaptive Self-Tuning Regulator (F-STR) is shown in Figure 3. The vector $e(t)$, depicted in Figure 3, is the state-error vector of order $4 \times 1$. It is evaluated as shown below.

$$e(t) = x(t) - x_{sp}(t) \tag{15}$$

such that, $\quad e(t) = \begin{bmatrix} e_\alpha(t) \\ e_\theta(t) \\ \dot{e}_\alpha(t) \\ \dot{e}_\theta(t) \end{bmatrix}, \quad x_{sp}(t) = \begin{bmatrix} \alpha(0) \\ -\pi \\ 0 \\ 0 \end{bmatrix}$

where, $x_{sp}(t)$ is the vector containing the set-point values of the state-variables. The adaptation procedure used in F-STR scheme is described as follows. At the beginning of a sampling instant, $t = T$, the proposed adaptation law acquires the updated values of state-error variables to re-compute the adjustable state-compensator gains, $K_f(t)$. Concurrently, the Zero-Order-Hold (ZOH) block shown on the channel

represented by the dashed line in Figure 3 also closes momentarily, at the beginning of the sampling instant, and holds the new values of $K_f(t)$. The updated values of $K_f(t)$ are transmitted ahead and used by the control law during the entirety of the sampling interval. When the next sampling instant begins, $t = T + 1$, the same process is repeated. The proposed gain-adaptation law is expressed below.

$$\dot{K}_f(t) = -F K_f(t) + G v(t) \tag{16}$$

such that, $\quad K_f(t) = \begin{bmatrix} k_\alpha(t) \\ k_\theta(t) \\ k_{\dot{\alpha}}(t) \\ k_{\dot{\theta}}(t) \end{bmatrix}, \quad F = \begin{bmatrix} \gamma_\alpha & 0 & 0 & 0 \\ 0 & \gamma_\theta & 0 & 0 \\ 0 & 0 & \gamma_{\dot{\alpha}} & 0 \\ 0 & 0 & 0 & \gamma_{\dot{\theta}} \end{bmatrix},$

$$G = \begin{bmatrix} \beta_\alpha & 0 & 0 & 0 \\ 0 & \beta_\theta & 0 & 0 \\ 0 & 0 & \beta_{\dot{\alpha}} & 0 \\ 0 & 0 & 0 & \beta_{\dot{\theta}} \end{bmatrix}, \quad v(t) = \begin{bmatrix} |e_\alpha(t)|^2 \\ |e_\theta(t)|^2 \\ e_\alpha(t).\dot{e}_\alpha(t) \\ e_\theta(t).\dot{e}_\theta(t) \end{bmatrix}$$
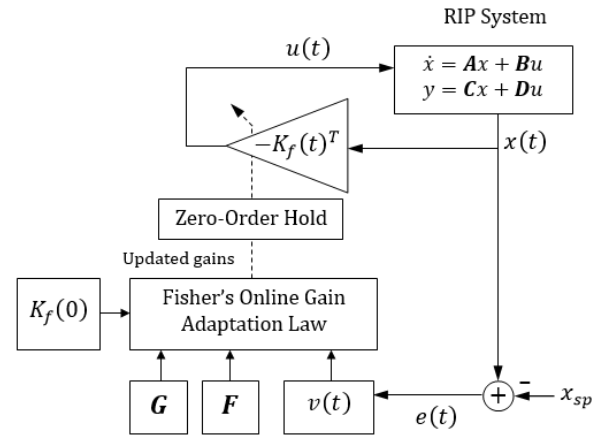


Fig. 3. The block diagram of the F-STR scheme.

where, $K_f(t)$ is a $4 \times 1$ vector containing the time-varying state-compensator gains, $v(t)$ is a vector containing the corresponding error-dependent terms used in each function. As shown in (16), the coefficients of the vector $v(t)$ are derived by appropriately combining the state-error variables provided by the vector $e(t)$. The matrix $F$ is a pre-defined positive-definite matrix whose coefficients are the decay-rates $\gamma_i$; where, '$i$' denotes the specific state-variable that is being referred to ($\alpha, \theta, \dot{\alpha}$, or $\dot{\theta}$). The matrix $G$ is a pre-defined positive-definite matrix whose coefficients are the gain-adaptation rates $\beta_i$. The gain-decay rate $\gamma_i$ decreases the rate-of-change of the corresponding gain exponentially under low error conditions in order to damp the oscillations, minimize control energy consumption, and prevent wind-up. The gain-adaptation rate $\beta_i$ enlarges the value of the corresponding gains as the state-error increases, and vice-versa. The F-STR mechanism captures the variations in the magnitude and direction of state-error variables to improve the system's response-speed and strengthen its damping. This arrangement flexibly manipulates the stiffness or softness of control effort as the response diverges or converges towards the reference, respectively (Balestrino et al., 2011). The said adaptation law is implemented in the control software by solving the differential equation in (16) as shown below.

$$K_f(t) = exp(-\boldsymbol{F}t)K_f(0) + \int_0^t \left( exp\big(-\boldsymbol{F}(t-p)\big)\boldsymbol{G}v(p) \right) dp \quad (17)$$

where, $exp(.)$ is the notation of the exponential function. The expression in (17) is mathematically programmed in the LabVIEW software simply by using the built-in functions and the Math-Script feature available in its Block-Diagram tool. The control block diagram in Figure 3 clearly manifests the adaptation behavior depicted in (17). The preset state-compensator vector $K_{lqr}$, identified in (14), is utilized as the initial vector $K_f(0)$ in (17). The initial conditions of the adaptation law are shown below.

$$K_f(0) = \begin{bmatrix} -6.21 \\ 130.56 \\ -4.22 \\ 17.83 \end{bmatrix}, \qquad v(t) = \begin{bmatrix} 0 \\ 0 \\ 0 \\ 0 \end{bmatrix} \quad (18)$$

As discussed earlier, at the beginning of every sampling interval, the control system computes the instantaneous values of the classical state-error and state-error derivatives by using the updated state-variables provided to it by the DAQ board. The updated error-variables are used by the adaptation law to re-compute and modify the values of the state-compensator gains in real-time. This process is repeated after every sampling interval. Thus, the vector $K_f(t)$ yields the updated values of the state-compensator gains after every sampling-interval. The coefficients of $\boldsymbol{F}$ and $\boldsymbol{G}$, $\gamma_i$ and $\beta_i$, must be positive to achieve the desired disturbance-rejection behavior without imposing large control input requirements. These parameters are tuned empirically by minimizing $J_2$ to yield the best position-regulation behavior. The selected values are shown in Table 2.

**Table 2. Tuned parameters of F-STR adaptation law.**

| Parameter | Range of selection | Tuned value |
|---|---|---|
| $\gamma_\alpha$ | [0, 1] | 0.035 |
| $\gamma_\theta$ | [0, 1] | 0.043 |
| $\gamma_{\dot\alpha}$ | [0, 1] | 0.013 |
| $\gamma_{\dot\theta}$ | [0, 1] | 0.021 |
| $\beta_\alpha$ | [0, 100] | 27.4 |
| $\beta_\theta$ | [0, 100] | 52.5 |
| $\beta_{\dot\alpha}$ | [0, 100] | 12.6 |
| $\beta_{\dot\theta}$ | [0, 100] | 22.8 |

The F-STR control law is expressed as follows.

$$u(t) = -K_f(t)^T x(t) \quad (19)$$

### 4.2. Nonlinearly-scaled MRAC (N-MRAC)

This section presents the formulation of an original self-tuning LQR augmented with a modified MRAC (Szidarovszky and Bahill, 1997; Kavuran et al., 2017). The conventional Model-Reference-Adaptive-System (MRAS) updates the gain vector online by minimizing the error between the outputs of the reference model, generated by the LQR, and the actual system (Ioannou and Fidan, 2006; Duka et al., 2007). The block diagram of the proposed Nonlinearly-scaled MRAC is shown in Figure 4. Consider the linear system expressed in (3). It is desired to construct an adaptive regulatory control law that manipulates the RIP system to imitate the response of the reference model expressed below (Chen, 2017).

$$\dot{x}_{ref}(t) = \boldsymbol{A}_{ref} x_{ref}(t) \quad (20)$$

The proposed adaptive regulatory control law is given by (21).

$$u(t) = -K_a(t)x(t) \quad (21)$$

where, $K_a(t)$ is the self-tuning gain vector that is dynamically updated via MRAS. The closed-loop representation of the actual system is given in (22).

$$\dot{x}(t) = (\boldsymbol{A} - \boldsymbol{B}K_a) x(t) = \boldsymbol{A}_c(K_a) x(t) \quad (22)$$

where, the matrix $\boldsymbol{A}_c$ depends on the vector $K_a$.
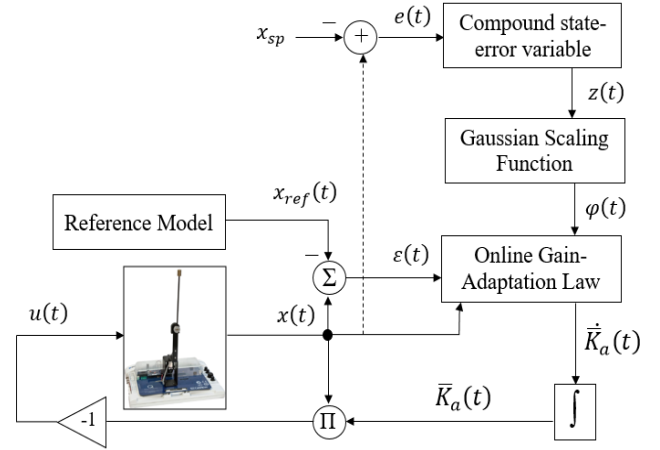


Fig. 4. The block diagram of the N-MRAC scheme.

*Compatibility condition*: Generally, it is not possible to acquire a vector $K_a$ such that the model described in (22) is equivalent to the reference model in (20). To establish a sufficient condition for tracking the reference-model, there exists a vector $\widehat{K}_a$ which is described as follows (Astrom and Wittenmark, 1995).

$$\boldsymbol{A}_c(\widehat{K}_a) = \boldsymbol{A}_{ref} = \boldsymbol{A} - \boldsymbol{B}\widehat{K}_a \quad (23)$$

This condition depicts that the columns of matrix $\boldsymbol{A} - \boldsymbol{A}_{ref}$ are linear combinations of the columns of the matrix $\boldsymbol{B}$. In this research, the $\boldsymbol{A}_{ref}$ is identified by taking $\widehat{K}_a = K_{lqr}$. Hence, the matrix $\boldsymbol{A}_{ref}$ is numerically expressed as follows.

$$\boldsymbol{A}_{ref} = \begin{bmatrix} 0 & 0 & 1 & 0 \\ 0 & 0 & 0 & 1 \\ 55.63 & -1147.18 & 37.51 & -159.72 \\ 14.27 & -263.82 & 9.62 & -40.97 \end{bmatrix} \quad (24)$$

The tracking-error-vector, $\varepsilon(t)$, computes the difference between the state-vectors of the actual system and the reference system. It is expressed as follows.

$$\varepsilon(t) = x(t) - x_{ref}(t) \quad (25)$$

The model-tracking-error decides the convergence rate of the adaptation mechanism. The total time-derivative of the tracking-error vector is given by (26).

$$\dot{\varepsilon}(t) = \dot{x}(t) - \dot{x}_{ref}(t) = \boldsymbol{A}x(t) + \boldsymbol{B}u(t) - \boldsymbol{A}_{ref}x_{ref}(t) \quad (26)$$

By simultaneously adding and subtracting the term $\boldsymbol{A}_{ref}x(t)$, on the right-hand side of equation (26), the expression of tracking-error-derivative is written as follows.

$$\dot{\varepsilon}(t) = Ax(t) + Bu(t) - A_{ref}x_{ref}(t) + A_{ref}x(t)$$
$$- A_{ref}x(t) \qquad (27)$$

The variables on the left-hand side can be manipulated to yield the following expression.

$$\dot{\varepsilon}(t) = A_{ref}\varepsilon(t) + \left(A - A_{ref} - BK_a(t)\right)x(t) \qquad (28)$$

By substituting the equation (23) in (28), the following expression is acquired.

$$\dot{\varepsilon}(t) = A_{ref}\varepsilon(t) + \left(B\widehat{K}_a - BK_a(t)\right)x(t)$$
$$= A_{ref}\varepsilon(t) + B\left(\widehat{K}_a - K_a(t)\right)x(t) \qquad (29)$$

The expression in (29) can also be expressed as follows.

$$\dot{\varepsilon}(t) = A_{ref}\varepsilon(t) - Bx(t)^T\left(K_a^{\ T}(t) - \widehat{K}_a^{\ T}\right) \qquad (30)$$

The expression in (30) is simplified as shown below.

$$\dot{\varepsilon}(t) = A_{ref}\varepsilon(t) + \delta\left(K_a^{\ T}(t) - \widehat{K}_a^{\ T}\right) \qquad (31)$$

such that,        $\delta = -Bx(t)^T$

It is assumed that the conditions needed for precise model tracking have been completely fulfilled while simplifying the expression of the tracking-error-derivative. The Lyapunov function, expressed in (32), is used to develop a stable online gain-adaptation law that modifies the values of $K_a(t)$ after every sampling interval.

$$V(\varepsilon, K_a) = \frac{1}{2}\left[\varphi\varepsilon(t)^T\overline{P}\varepsilon(t) \right.$$
$$\left. + \left(K_a^{\ T}(t) - \widehat{K}_a^{\ T}\right)^T\left(K_a^{\ T}(t) - \widehat{K}_a^{\ T}\right)\right] (32)$$

where, $\overline{P}$ is a positive definite matrix and $V(e, K_a)$ is positive semi-definite matrix. The parameter $\varphi$ is the preset positive adaptation-gain. The matrix $\overline{P}$ is calculated as follows.

$$A_{ref}^T\overline{P} + \overline{P}A_{ref} = -Q \qquad (33)$$

The $Q$ matrix, identified in (13), is used to solve the equation (33). Following the mathematical property in (33), there would always exist a pair of positive definite matrices, $\overline{P}$ and $Q$, if $A_{ref}$ is stable. The derivative of $V(.)$ is given in (34).

$$\dot{V}(\varepsilon, K_a) = -\frac{1}{2}\varphi\varepsilon(t)^T Q\varepsilon(t)$$
$$+ \left(K_a^{\ T}(t) - \widehat{K}_a^{\ T}\right)^T\left(\dot{K}_a^{\ T}(t) + \varphi\delta^T\overline{P}\varepsilon(t)\right) \quad (34)$$

For $\dot{V}(\varepsilon, K_a)$ to be negative-definite, the expression in (35) is chosen as the online gain adjustment law.

$$\dot{K}_a^{\ T}(t) = -\varphi\delta^T\overline{P}\varepsilon(t) \qquad (35)$$

This expression proves that $\varepsilon(t)$ will eventually converge to zero. The simplified expression of the gain adjustment law is given in (36).

$$\dot{K}_a(t) = \left(\varphi x(t)B^T\overline{P}\varepsilon(t)\right)^T \qquad (36)$$

where, $\overline{P}$ is a matrix of order $4\times4$, $x(t)$ and $\varepsilon(t)$ are vectors of order $4\times1$, and $B^T$ is a $1\times4$ order vector. The matrix $\overline{P}$ and

vector $B^T$ are available a priori. Correspondingly, $\dot{K}_a$ is evaluated as a $1\times4$ order vector. The adaptation-gain, $\varphi$, directly influences the convergence-rate and sensitivity of the gain adjustment law. The dependence of gain-adjustment law on the adaptation-gain varies with respect to the changes in the system's state-error, which enhances the adaptability of the control system. Under perturbed situations, a higher value of adaptation-gain is selected for quick convergence of adaptation-gains due to the rapid variations occurring in the system's states. During steady-state conditions, a lower adaptation-gain is required to render soft control effort due to the gentle state-variations. A larger adaptation-gain during disturbed conditions minimizes the transient recovery time, whereas a smaller adaptation-gain during steady-state conditions damps the steady-state fluctuations. The fixed value of adaptation-gain lacks the flexibility to efficiently manipulate the softness or stiffness of the control-input trajectory under the ever-changing state-variables.

In this research, a smooth transitioning mechanism is employed that enables the MRAS to automatically commute between different linear controllers, after every sampling interval, to stabilize the RIP under steady-state as wells as the disturbed-state. For this purpose, a pre-calibrated state-error-dependent nonlinear-scaling function is employed that smoothly increases the adaptation-gain for large magnitudes of state-error, and vice versa. The zero-mean Gaussian function is selected because it is symmetrical, continuous, and bounded. The proposed state-error-dependent Gaussian-Scaling-Function (GSF) is formulated as shown below.

$$\varphi(t) = \varphi_{ds} - (\varphi_{ds} - \varphi_{ss})exp(-\mu|z(t)|^2) \qquad (37)$$

where, $\mu$ is the preset variation-rate of the GSF. The parameters $\varphi_{ds}$ and $\varphi_{ss}$ are the adaptation-gains associated with the steady-state and the disturbed-state of RIP, respectively. The input of the GSF is the compound state-error variable, $z(t)$, which is computed as the linear weighted sum of the system's state-error variables, as shown below.

$$z(t) = \sigma_1 e_\alpha(t) + \sigma_2 e_\theta(t) + \sigma_3\dot{e}_\alpha(t) + \sigma_4\dot{e}_\theta(t) \qquad (38)$$

where, $\sigma_1$, $\sigma_2$, $\sigma_3$, and $\sigma_4$ are the predetermined weightages associated with each state-error variable. This expression unifies all the state-error variables of the RIP system into one equation and delivers a single variable, $z(t)$, that informs the control system regarding the overall impact of exogenous disturbance(s). The weightages are selected empirically such that a stiffer control effort is delivered when the time-domain response is diverging from the reference and a softer control effort is delivered when the response is converging. The waveform of the proposed GSF is shown in Figure 5. The hyper-parameters associated with the GSF are tuned empirically by minimizing the cost function $J_2$ to deliver a time-optimal control effort. The range-space as well the optimized value of each parameter are provided in Table 3. The augmentation of the MRAC with a self-adjusting adaptation-gain allows it to efficiently compensate the state deviations as the system transits from steady-state to disturbed-state, and vice versa. The modified online gain adjustment law is presented in (39).

$$\dot{\overline{K}}_a(t) = \left(\varphi(t)x(t)B^T\overline{P}\varepsilon(t)\right)^T \qquad (39)$$

The gain adaptation law is implemented in the control software by programming the expression given in (40).

$$\overline{K}_a(t) = \overline{K}_a(0) + \int_0^t \left(\varphi(t)x(t)B^T\overline{P}\varepsilon(t)\right)^T dt \qquad (40)$$

The fixed-gain vector $K_{lqr}$, identified in (14), is utilized as the $\overline{K}_a(0)$ in (40). The Nonlinearly-scaled MRAC (N-MRAC) law is expressed in (41).
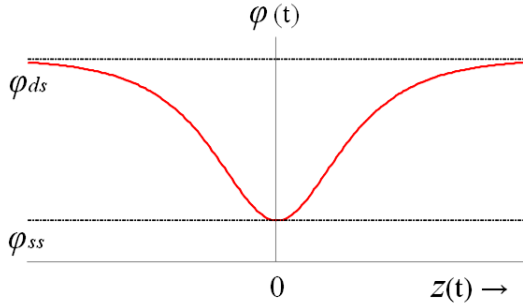
$$u(t) = -\overline{K}_a(t)x(t) \qquad (41)$$



Fig. 5. The waveform of the proposed GSF.

**Table 3. Parameter selection of the GSF.**

| Parameter | Range | Tuned value |
|---|---|---|
| $\varphi_{ds}$ | [0, 5] | 2.04 |
| $\varphi_{ss}$ | [0, 5] | 0.11 |
| $\mu$ | [0, 10] | 7.85 |
| $\sigma_1$ | [-10, 10] | -0.72 |
| $\sigma_2$ | [-10, 10] | 2.25 |
| $\sigma_3$ | [-10, 10] | -0.28 |
| $\sigma_4$ | [-10, 10] | 0.78 |

The flow chart of the algorithm used to realize the proposed N-MRAC scheme is illustrated in Figure 6.

## 5. EXPERIMENTAL SETUP

This section presents the experimental evaluation of the proposed adaptive control strategies via hardware-in-the-loop experiments conducted on the QNET RIP setup.
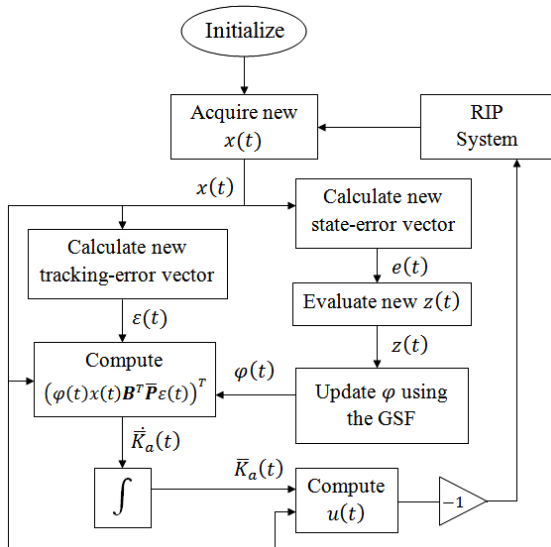


Fig. 6. The flow-chart of the N-MRAC algorithm.

### 5.1. Experimental Evaluation

The hardware setup of the QNET RIP system is shown in Figure 7. The performance of N-MRAC is compared with the LQR and F-STR via four unique test-cases that are designed to analyze the position-regulation and disturbance-rejection behavior of each controller in the physical environment. The following limitations associated with the interface signals of the QNET RIP system are considered during the experimental trials.

- Rod displacement limit: $|e_\theta(t)| < 0.07$ rad.

- Arm displacement limit: $|e_\alpha(t)| < 2.97$ rad.

- Control input limit: $|V_m(t)| < 20.0$ V.

The limitations of $e_\theta$, $e_\alpha$, and $V_m$ defined above are experimentally identified. Owing to the pendulum dynamics, the rod collapses if $e_\theta$ exceeds the defined range. Similarly, if $e_\alpha$ violates the defined range, the power-chord and data-cable of the rotary encoder coupled with the rod's pivot obstruct the rotational movement of the arm causing the rod to collapse. The control input is kept within ±20.0 V to avoid over-heating or unnecessary wear-and-tear of the motor's winding. The pendulum rod is erected manually and stabilized at the beginning of every experimental trial. Approximately, the same initial condition are ensured at the beginning of every trial. The sampling-time of the zero-order-hold used in the F-STR is set at 1.0 ms. In order to simplify the visualization, the angular responses are deliberately shown in degrees (deg.). The hardware-in-the-loop structure is shown in Figure 8. The control software block diagram is shown in Figure 9. The details of the four experimental tests are presented below.
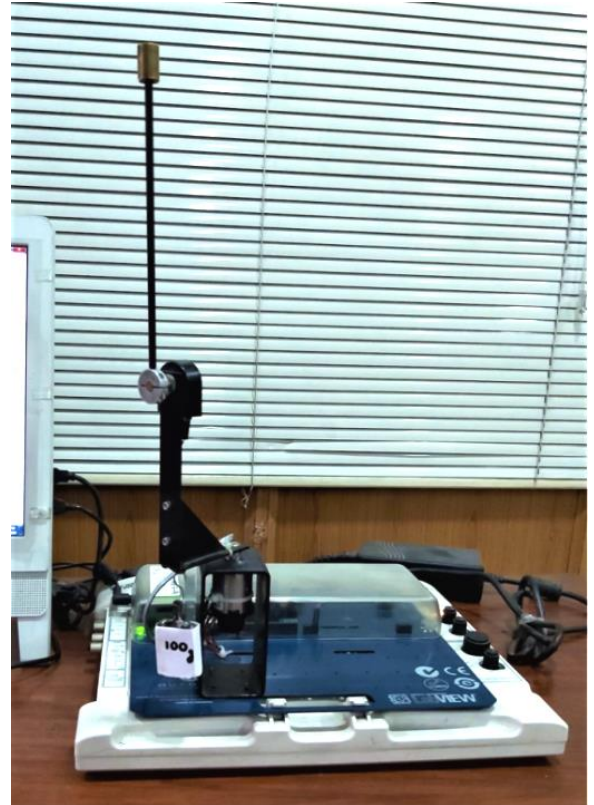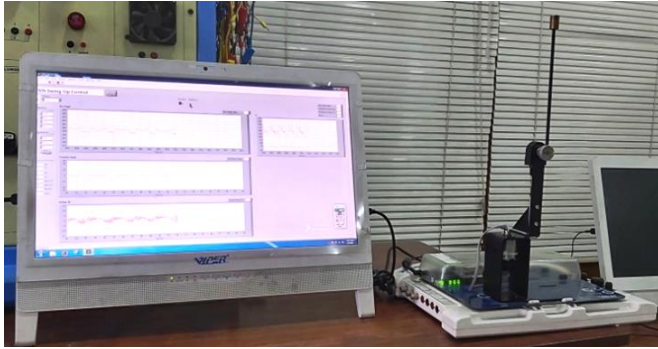


Fig. 7. The QNET RIP system used for experimentation.

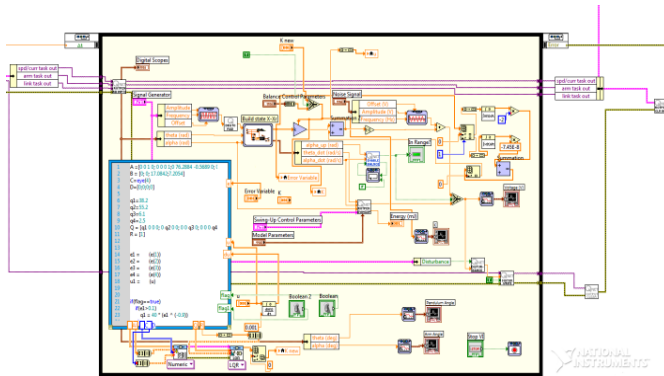Fig. 8. The hardware-in-the-loop structure of the RIP setup.



Fig. 9. The LabVIEW control software block diagram.

***A. Position-regulation behavior:*** This test is conducted to observe the system's position-regulation behavior and control energy consumption under nominal conditions and in the absence of any bounded exogenous disturbances. The objective is to vertically stabilize the pendulum rod with minimum deviations while making sure that the arm tracks its initial position. The position-regulation response and the corresponding control input profile of each control system are graphically illustrated in Figures 10, 11, and 12, respectively. The state-compensator gain variations exhibited by F-STR and N-MRAC are shown in Figures 13 and 14, respectively.

***B. Impulsive-disturbance rejection:*** The robustness of each control system against the bounded exogenous disturbances is examined by injected a pulse in the control-input signal at t ≈ 1.5 s. The magnitude and duration of the applied pulse are - 10.0 V and 0.1 s, respectively. The behavior of each control system is illustrated in Figures 15, 16, and 17, respectively. The state-compensator gain variations exhibited by F-STR and N-MRAC are shown in Figures 18 and 19, respectively.
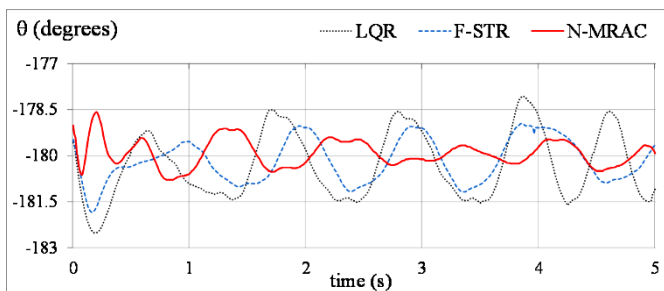


Fig. 10. Pendulum angle response under normal conditions.
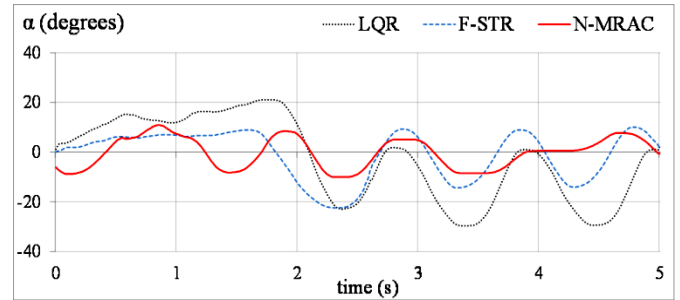


Fig. 11. Arm angle response under normal conditions.
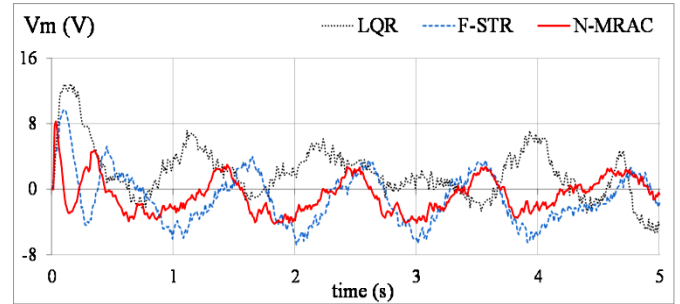


Fig. 12. Control voltage response under normal conditions.
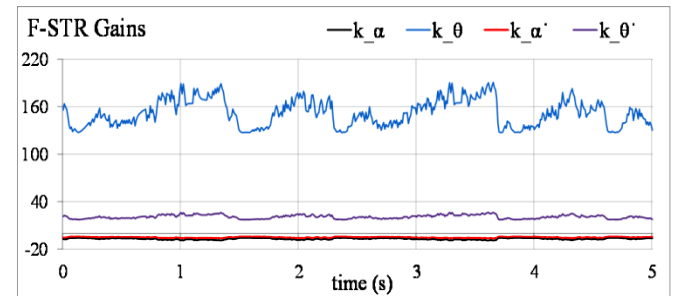


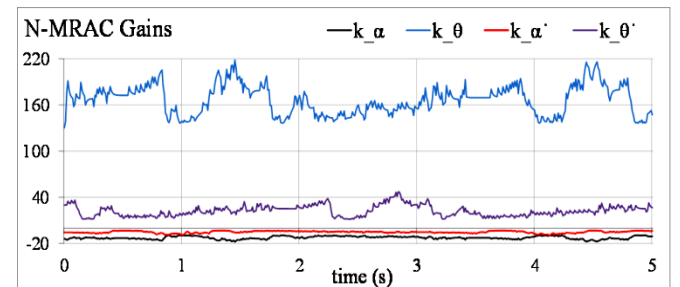Fig. 13. F-STR gains under normal conditions.


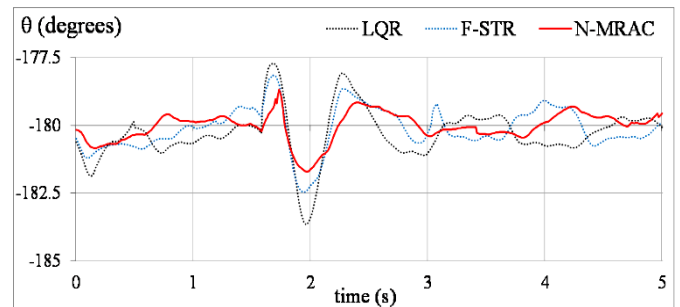
Fig. 14. N-MRAC gains under normal conditions.



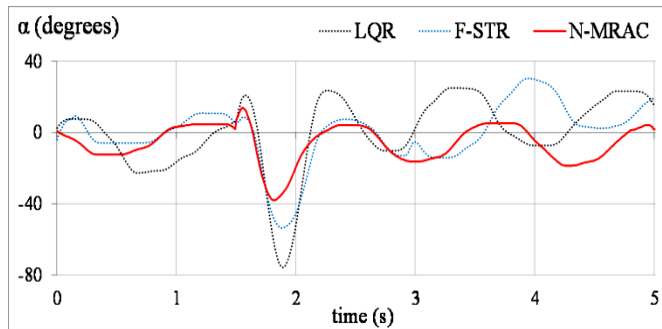Fig. 15. Pendulum angle response under pulse disturbance.

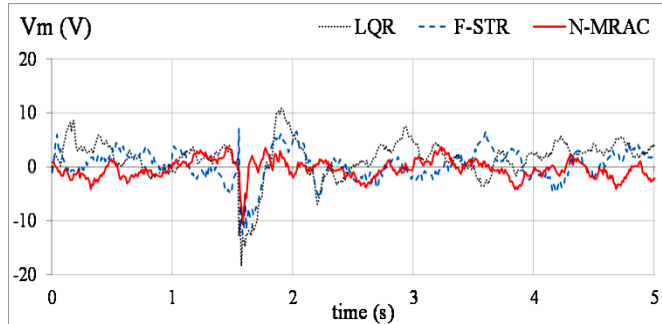Fig. 16. Arm angle response under pulse disturbance.



Fig. 20. Pendulum angle response under white noise.


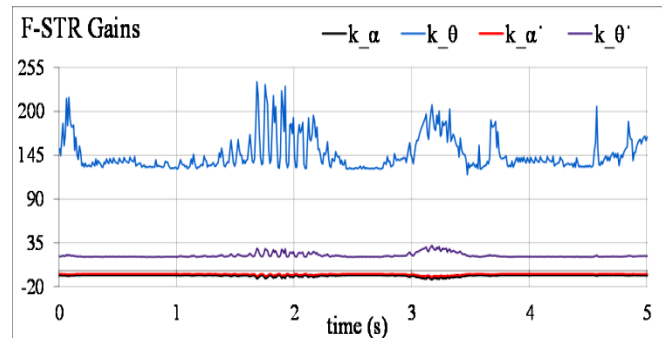
Fig. 17. Control voltage response under pulse disturbance.



Fig. 21. Arm angle response under white noise.



Fig. 18. F-STR gains under pulse disturbance.



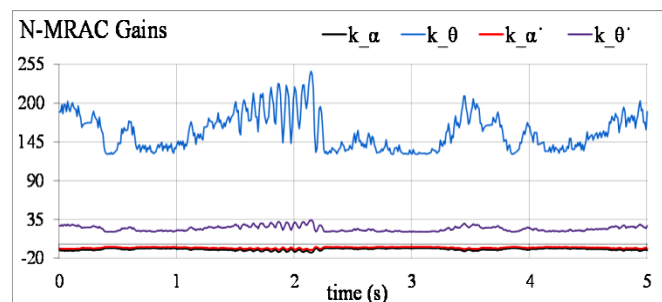Fig. 22. Control voltage response under white noise.



Fig. 19. N-MRAC gains under pulse disturbance.
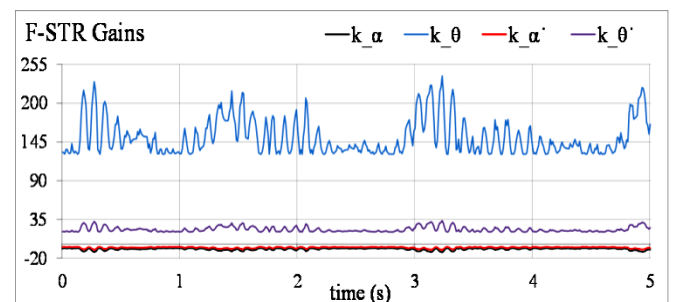


Fig. 23. F-STR gains under white noise.

*C. Noise attenuation:* The control system's immunity against the detrimental effects of measurement noise (or mechanical vibrations) is evaluated by adding a band-limited white noise signal directly in the system's control-input signal. The injected signal has a noise power of $0.5 \times 10^{-3}/(rad/s)$ and sampling time of 0.1 s. The resulting fluctuations observed in the time-domain response of each control system are depicted in Figures 20, 21, and 22, respectively. The state-compensator gain variations exhibited by F-STR and N-MRAC are shown in Figures 23 and 24, respectively.
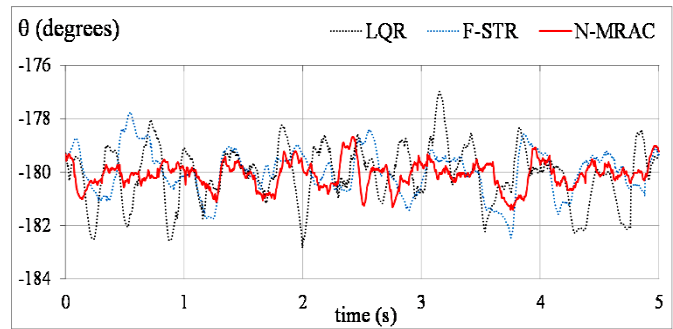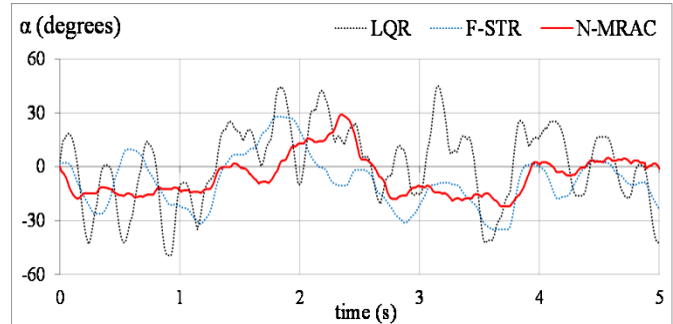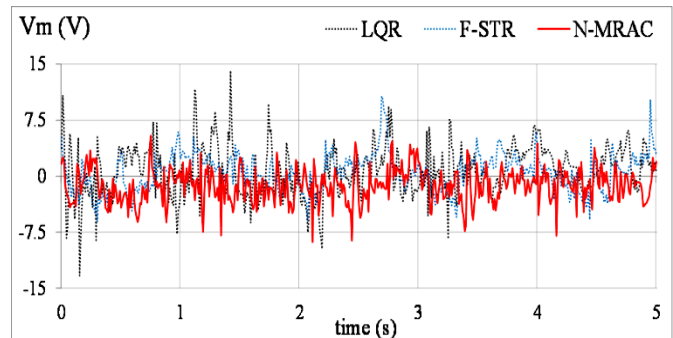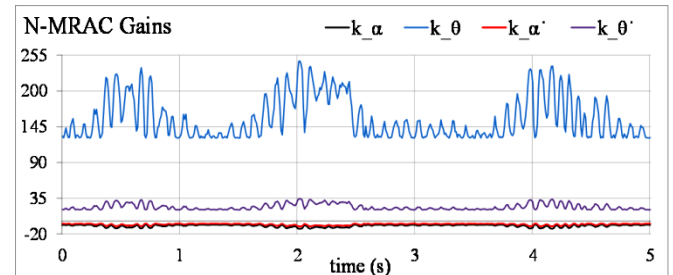


Fig. 24. N-MRAC gains under white noise.

**D. *Modeling-error compensation:*** The control system's immunity against modeling-errors is assessed by introducing a step-increment in $R_m$ via the mechanism shown in Figure 25. As shown in Table 1, the standard value of $R_m$ is 3.30 Ω. Initially, the RIP is balanced under nominal conditions. At t ≈ 1.5 s, a 1.0 Ω resistor is connected in series with the motor terminals by changing the position of the selector-switch, shown in Figure 25, from A to B. The value of the external resistance is approximately one-third that of the motor's armature resistance, $R_m$. This modification permanently alters the coefficients of the state-space matrices. This abrupt model variation introduces perturbations in the response. The interfacing of this circuit with the electronic motor-driver of the QNET RIP setup is shown in Figure 26. The resulting state and control-input variations of each control system are graphically illustrated in Figures 27, 28, and 29, respectively. The state-compensator gain variations exhibited by F-STR and N-MRAC are shown in Figures 30 and 31, respectively.
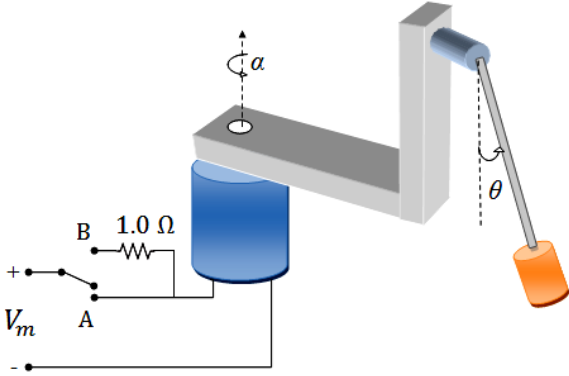


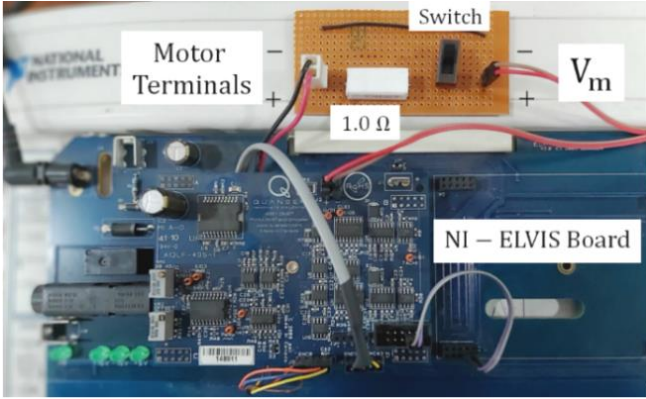Fig. 25. Schematic of the modified RIP setup.



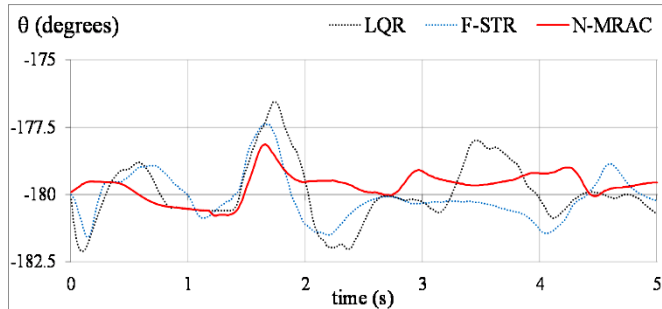Fig. 26. Schematic of the modified RIP setup.



Fig. 27. Pendulum angle response under modeling-error.
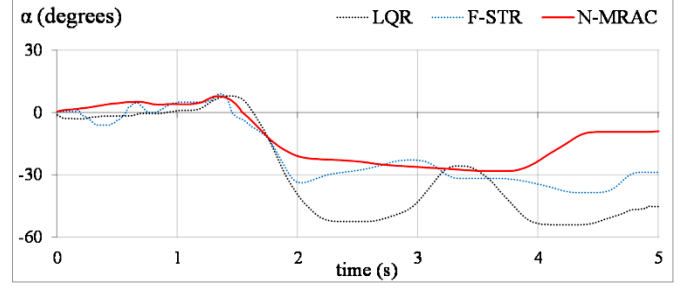


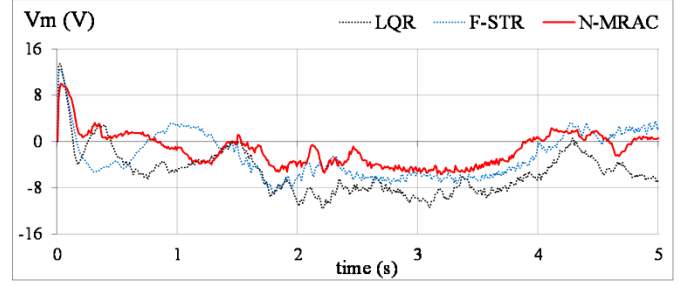Fig. 28. Arm angle response under modeling-error.



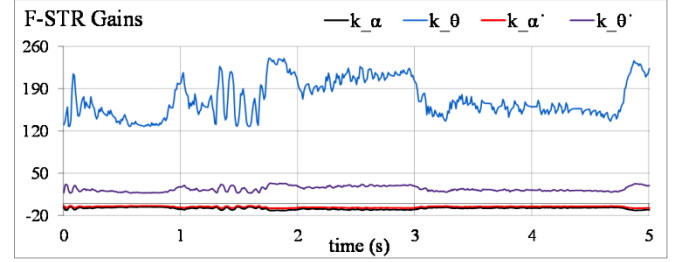Fig. 29. Control voltage response under modeling-error.



Fig. 30. F-STR gains under modeling-error.
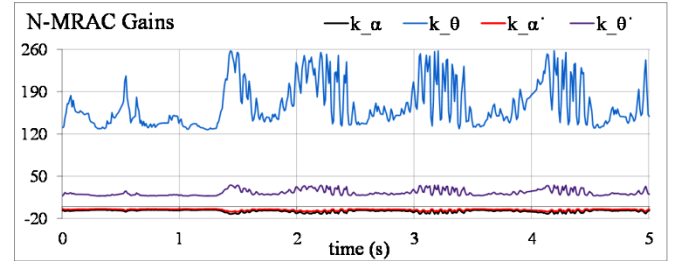


Fig. 31. N-MRAC gains under modeling-error.

*5.2. Analysis and Discussions*

The performance analysis is done in terms of the standard performance indicators. These indicators include the root-mean-squared value of state-error (RMSE$_x$) in degrees, the absolute value of peak overshoot or undershoots (M$_{p,x}$) under transient disturbances, the time taken by the response to settle within ±2% of the reference value (t$_{s,x}$), the average control power evaluated in terms of mean-squared-value of the motor control voltage (MSV$_m$), and the peak control voltage (V$_{m,p}$) in the control profile under transient disturbances. The comparative performance assessment of the experimental results is summarized in Table 4. The results clearly validate the superior robustness of the N-MRAC against bounded exogenous disturbances and modeling errors.

In Test-A, the angular responses of LQR exhibit persistent fluctuations around the reference angles. The angular

responses of F-STR converge relatively faster to reference than the LQR, with a relatively lesser amplitude of oscillations in the equilibrium position. The N-MRAC exhibits the most time-optimal control effort. The arm and rod-angle quickly converge to the reference angles and track them with minimal steady-state fluctuations. In Test-B, the N-MRAC response exhibits rapid transits with reasonable damping to compensate for the effects of impulsive disturbances. The N-MRAC demonstrates the minimum magnitude of $M_p$ as well as $t_{rec}$ after recovering from the transient disturbance. In Test-C, the arm and rod vibrate persistently throughout the trial when the system is equipped with LQR. The responses yielded by F-STR also exhibit persistent oscillations throughout the time-window with a relatively lesser magnitude of RMSE. The N-MRAC effectively attenuates the influence of noise signal and manifests minimum RMSE magnitudes in the angular responses of arm and pendulum. In Test-D, the N-MRAC robustly compensates for the modeling-error. It overcomes the induced parametric variations in minimum time while effectively damping the fluctuations around the reference angle. The modification in the value of $R_m$ reduces the time-constant and the transfer coefficient of the motor's coil circuit by approximately 23.3%. This leads to an abrupt increment in the electrical inertia which inevitably increases the control energy consumption. The control effort delivered by the control software, to reject the bounded exogenous disturbances, leads to abrupt changes in the direction of motor rotation which induces chattering in the arm and rod angle responses.

**Table 4. Summary of experimental results.**

| Test | Indicators | Control system | | |
|------|-----------|------|------|------|
| | | LQR | F-STR | N-MRAC |
| **A** | $RMSE_\theta$ (deg.) | 2.05 | 1.26 | 0.68 |
| | $RMSE_\alpha$ (deg.) | 16.61 | 9.76 | 6.13 |
| | $MSV_m$ ($V^2$) | 14.97 | 10.14 | 5.33 |
| **B** | $RMSE_\theta$ (deg.) | 2.32 | 1.62 | 0.86 |
| | $|M_{p,\theta}|$ (deg.) | 3.66 | 2.46 | 1.75 |
| | $t_{s,\theta}$ (s) | 1.55 | 1.26 | 1.21 |
| | $RMSE_\alpha$ (deg.) | 20.84 | 16.68 | 11.87 |
| | $|M_{p,\alpha}|$ (deg.) | 75.86 | 53.66 | 38.02 |
| | $t_{s,\alpha}$ (s) | 1.54 | 1.19 | 1.15 |
| | $MSV_m$ ($V^2$) | 15.42 | 8.63 | 4.70 |
| | $V_{m,p}$ (V) | -18.42 | -12.61 | -10.70 |
| **C** | $RMSE_\theta$ (deg.) | 2.21 | 1.76 | 1.02 |
| | $RMSE_\alpha$ (deg.) | 19.56 | 17.47 | 11.44 |
| | $MSV_m$ ($V^2$) | 13.83 | 10.17 | 6.72 |
| **D** | $RMSE_\theta$ (deg.) | 2.17 | 1.77 | 0.92 |
| | $RMSE_\alpha$ (deg.) | 36.58 | 25.09 | 17.84 |
| | $MSV_m$ ($V^2$) | 40.17 | 21.66 | 10.56 |

Despite this inevitable behavior, the results show that the proposed control system effectively minimizes the ripple content in the time-domain responses. Furthermore, the on-board DC motor-driver circuit is commercially designed, by QNET, with sufficient agility to safely handle and withstand the discontinuous control activity during the experiments.

In Section 4.2, the stability of N-MRAC has been investigated in the simplified hypothesis of the continuous time system;

although N-MRAC is a discrete time system. However, the result has been also valid in the experimental part, where the sampling time used to implement the compensator $\overline{K}_a(t)$ was 1.0 ms. Furthermore, the superior disturbance-rejection capability exhibited by N-MRAC is attributed to the enhanced adaptability of the state-compensator gains, rendered by the self-adjusting adaptation-gains in the MRAC law. This arrangement significantly improves the response-speed of the control system and efficiently compensates the detrimental effects of bounded exogenous disturbances.

The performance of the proposed N-MRAC is compared with the results reported in previous works; where in, the QNET RIP system is stabilized via a self-tuning dual fractional-PD controller in (Saleem and Mahmood-ul-Hasan, 2019), an adaptive LQR with an adjustable control weighting-factor in (Saleem et. al., 2020), and an adaptive LQR with adjustable state and control weighting-factors in (Saleem and Mahmood-ul-Hasan, 2021). These controllers are denoted as SDFPD, SRLQR, and H-STR in the literature, respectively. Only two testing scenarios are common among the prescribed control systems; namely, performance under normal conditions and impulsive disturbances. Hence, only these scenarios are discussed here. Under normal conditions, the arm position-regulation accuracy exhibited by N-MRAC is better than that of SRLQR, consistent with that of H-STR, and poorer than that of SDFPD. Moreover, the control energy consumption of N-MRAC is relatively lesser than that of both H-STR and SRLQR, but higher than that of SDFPD. Under impulsive disturbances, the N-MRAC shows an $|M_{p,\theta}|$ of only 1.75 deg. (See Table 4) for a -10.0 V pulse injected in the control signal, which is almost twice in magnitude than the pulse signals used to conduct the similar tests for SRLQR, H-STR, and SDFPD. Hence, the impulsive-disturbance-rejection capability of N-MRAC is fairly consistent with the aforementioned strategies.

6. CONCLUSION

This paper presents the systematic formulation of an enhanced adaptive stabilization control strategy for the RIP systems by employing an innovative state-error-dependent self-tuning mechanism. Two online self-adaptive control strategies are comparatively analyzed; namely, the Fisher-adaptive gain-adjustment law as well as nonlinearly-scaled MRAS. Each gain-adjustment mechanism is methodically synthesized. The F-STR reasonably mitigates the effects of external disturbances and modeling-errors encountered by the system. However, to further enhance the control system's adaptability and robustness against nonlinear disturbances, a modified MRAC is employed. The adaptation-gain of the Lyapunov gain-adjustment law, associated with the MRAC, is dynamically adjusted online via a pre-configured state-error dependent Gaussian scaling function. The mutation of MRAS via the smooth nonlinear scaling function significantly improves the pendulum's transient recovery speed and strengthens its damping against fluctuations. The superior robustness of N-MRAC is validated by conducting credible experiments on the QNET Rotary Pendulum Board and analyzing the corresponding results in comparison with other control system variants. The stability of the N-MRAC has been investigated in the simplified hypothesis of the continuous time system; although N-MRAC is a discrete time system.

However, the result has been also valid in the experimental analysis, where the sampling time used to implement the compensator $\overline{K}_a(t)$ was 1.0 ms. There is plenty of room for future enhancements. The robustness of the proposed control strategy can be investigated by applying it to control other classes of under-actuated mechatronic systems. Moreover, the artificial-immune self-tuning strategy can also be examined for the online modification of the adaptation-gain of the MRAC system, to ensure a flexible state-compensator gain variation in stabilization control applications. Finally, in the future, the performance of N-MRAC must be assessed under sinusoidal disturbances and arm-mass variations in real-time.

## REFERENCES

Ashrafiuon, H., and Whitman, A.M. (2011). Closed-loop dynamic analysis of a rotary inverted pendulum for control design. *Journal of DynamicSystems, Measurement, and Control*, 134(2), pp. 1-9.

Astrom, K.J., and Wittenmark, B. (1995). *Adaptive Control*. 2nd ed. Pearson Education, London, UK.

Balamurugan, S., Venkatesh, P., and Varatharajan, M. (2017). Fuzzy sliding-mode control with low pass filter to reduce chattering effect: an experimental validation on Quanser SRIP. *Sadhana*, 42(10), pp. 1693–1703.

Balestrino, A., Biagini, V., Bolognesi, P., and Crisostomi, E. (2009). Advanced Variable Structure PI controllers. In: *Proceedings of IEEE Conference on Emerging Technologies & Factory Automation*, Mallorca, Spain, 22-25 September 2009, pp. 1-8.

Balestrino, A., Caiti, A., Calabr, V., Crisostomi, E., and Landi, A. (2011). *Chaper 5 - From Basic to Advanced PI Controllers: A Complexity vs. Performance Comparison* In: Advances in PID Control, V.D. Yurkevich (Ed.), Intech, Rijeka, Croatia, pp. 85–100.

Bhatti, O.S., Mehmood-ul-Hasan, K., and Imtiaz, M.A. (2015). Attitude Control and Stabilization of a Two-Wheeled Self-Balancing Robot. *Control Engineering and Applied Informatics*, 17(3), pp. 98-104.

Bhatti, O.S., Tariq, O.S., Manzar, A., and Khan, O.A. (2018). Adaptive intelligent cascade control of a ball-riding robot for optimal balancing and station-keeping. *Advanced Robotics*, 32(2), pp. 63-76

Boubaker, O. (2013). The inverted pendulum benchmark in nonlinear control theory: a survey. *International Journal of Advanced Robotic Systems*, 10(5), pp. 233–242.

Chen, K.Y. (2017). Model reference adaptive minimum-energy control for a mechatronic elevator system. *Optimal Control Applications and Methods*, 38(1), pp. 3–18.

Cuong, N.D., Lanh, N.V., and Huyen, D.V. (2013). Design of MRAS-based adaptive control systems, In: *Proceedings of International Conference on Control, Automation and Information Sciences*, Nha Trang, Vietnam, 25-28 Nov. 2013, pp. 79-84.

Duka, A.D., Oltean, S.E., and Dulău, M. (2007). Model reference adaptive vs. learning control for the inverted pendulum. A comparative case study. *Control Engineering and Applied Informatics*, 9(4), pp. 67-75.

Fisher, A.D., VanZwieten, J.H., and VanZwieten, T.S. (2009). Adaptive Control of Small Outboard-Powered Boats for Survey Applications. In: *OCEANS'09 Proceedings of the MTS/IEEE Marine Technology for Our Future: Global and Local Challenges*, Biloxi, Mississippi, 26-29 October 2009, pp. 1-9.

Ghartemani, M.K., Khajehoddin, S.A., Jain, P., Bakhshai, A. (2011). Linear quadratic output tracking and disturbance rejection. *International Journal of Control*, 84(8), pp. 1442-1449.

Gritli, H., and Belghit, S. (2018). Robust feedback control of the underactuated Inertia Wheel Inverted Pendulum under parametric uncertainties and subject to external disturbances: LMI formulation. *Journal of Franklin Institute*, 355(18), pp. 9150-9191.

Hanwate, S., Hote, Y.V., and Budhraja, A. (2019). Design and implementation of adaptive control logic for cart-inverted pendulum system. *Proceedings of the Institute of Mechanical Engineers, Part I: Journal of Systems and Control Engineering*, 233(2), pp. 164-178.

Hassanzadeh, A., Nejadfard, A., and Zadi, M.(2011). A Multivariable Adaptive Control Approach for Stabilization of a Cart-Type Double Inverted Pendulum. *Mathematical Problems in Engineering*, 2011, Article ID 970786.

Ioannou, P.A., and Fidan, B. (2006). *Adaptive Control Tutorial*. In: Advances in Design and Control. SIAM, PA, USA.

Jian, Z., and Yongpeng, Z. (2011). Optimal Linear Modeling and its Applications on Swing-up and Stabilization Control for Rotary Inverted Pendulum, *Proceedings of the 30th Chinese Control Conference*, Yantai, China, July 22-24, 2011; IEEE: pp. 493-500.

Kavuran, G., Ates, A., Alagoz, B.B., and Yeroglu, C. (2017). An Experimental Study on Model Reference Adaptive Control of TRMS by Error-Modified Fractional Order MIT Rule. *Control Engineering and Applied Informatics*, 19(4), pp. 101-111.

Li, Z., Yang, C., and Fan, L. (2013). *Advanced Control of Wheeled Inverted Pendulum Systems*. Springer, London.

Lewis, F.L., Vrabie, D., and Syrmos, V.L. (2012). *Optimal Control*. John Wiley and Sons, New Jersey.

Mahmoud, M.S. (2018). *Advanced Control Design with Application to Electromechanical Systems*. 1st Ed., Elsevier Science, New York.

Nguyen, N.P., Oh, H., Kim, Y., and Moon, J. (2021). A nonlinear hybrid controller for swinging-up and stabilizing the rotary inverted pendulum. *Nonlinear Dynamics*, pp. 1 - 21. https://doi.org/10.1007/s11071-021-06317-2

Okyere, E., Bousbaine, A., Poyi, G.T., Joseph, A.K., and Andrade, J.M. (2019). LQR controller design for quad-rotor helicopters. *The Journal of Engineering*, 17(6), pp. 4003 – 4007.

Prasad, L.B., Tyagi, B., and Gupta, H.A. (2014). Optimal Control of Nonlinear Inverted Pendulum System Using PID Controller and LQR: Performance Analysis Without and With Disturbance Input. *International Journal of Automation and Computing*, 11(6), pp. 661–670.

Quanser. (2009). QNET Rotary Pendulum Trainer – Student Manual. Quanser Inc,

Saleem, O., and Mahmood-ul-Hasan, K. (2019). Robust stabilisation of rotary inverted pendulum using

intelligently optimised nonlinear self-adaptive dual fractional order PD controllers. *International Journal of Systems Science*, 50(7), pp. 1399-1414.

Saleem, O., Mahmood-ul-Hasan, K., and Rizwan, M. (2020). Self-Tuning State-Feedback Control of Rotary Pendulum via Online Adaptive Reconfiguration of Control Penalty-Factor. *Control Engineering and Applied Informatics*, 22(4), pp. 23-33.

Saleem, O., and Mahmood-ul-Hasan, K. (2021). Adaptive State-space Control of Under-actuated Systems Using Error-magnitude Dependent Self-tuning of Cost Weighting-factors. *International Journal of Control, Automation and Systems*, 19(2), pp. 931-941.

Sefriti, S., Boumhidi, J., Naoual, R., and Boumhidi, I. (2012). Adaptive Neural Network Sliding Mode Control For Electrically-Driven Robot Manipulators. *Control Engineering and Applied Informatics*, 14(4), pp. 27-32.

Subramaniana, R.G., and Elumalai, V.K. (2016). Robust MRAC augmented baseline LQR for tracking control of 2 DoF helicopter. *Robotics and Autonomous Systems*, 86, pp. 70–77.

Sukontanakarn, V., and Parnichkun, M.(2009). Real-Time Optimal Control for Rotary Inverted Pendulum, *American Journal of Applied Sciences*, 6(6), pp. 1106-1115.

Szidarovszky, F., and Bahill, A.T. (1997). *Linear Systems Theory*. 2nd ed. CRC Press, FL, USA.

Szuster, M., and Hendzel, Z. (2017). *Intelligent optimal adaptive control for mechatronic systems, Studies in Systems, Decision and Control*. Springer, Berlin, Germany.

Ullah, S., Khan, Q., Mehmood, A., and Akmeliawati, R. (2019). Integral backstepping based robust integral sliding mode control of underactuated nonlinear electromechanical systems. *Control Engineering and Applied Informatics*, 21(3), pp. 42-50.

Yu, H. Liu, Y., and Yang, T.(2008). Closed-loop tracking control of a pendulum-driven cart-pole underactuated system. *Proceedings of the Institute of Mechanical Engineers, Part I: Journal of Systems and Control Engineering*, 222(2), pp. 109–125.

Zhang, H., Wang, J.,and Lu, G. (2014). Self-organizing fuzzy optimal control for under-actuated systems. *Proceedings of the Institute of Mechanical Engineers, Part I: Journal of Systems and Control Engineering*, 228(8), pp. 578-590.